JOURNAL OF PROPULSION AND POWER
Vol. 13, No. 5, September–October 1997

# High-Temperature Braided Rope Seals for Static Sealing Applications

Bruce M. Steinetz*
*NASA Lewis Research Center, Cleveland, Ohio 44135*
Michael L. Adams†
*Modern Technologies Corporation, Middleburg Heights, Ohio 44130*
Paul A. Bartolotta‡
*NASA Lewis Research Center, Cleveland, Ohio 44135*
Ram Darolia§
*General Electric, Cincinnati, Ohio 45215*
and
Andrew Olsen¶
*General Electric, Lynn, Massachusetts 01910*

**Achieving efficiency and performance goals of advanced aircraft and industrial systems is leading designers to implement high-temperature materials such as ceramics and intermetallics. Generally, these advanced materials are applied selectively in the highest temperature sections of the engine system, including the combustor and high-pressure turbine sections, among others. Thermal strains that result in attaching the low expansion-rate components to high expansion-rate superalloy structures can cause significant life reduction in the components. Seals are being designed to both seal and serve as compliant mounts, allowing for relative thermal growths between high-temperature, but brittle, primary structures and the surrounding support structures. Designers require high-temperature, low-leakage, compliant seals to mitigate thermal stresses, and to control parasitic and cooling airflow between structures. High-temperature braided rope seals are being developed in a variety of configurations to help solve these problems. This paper will describe the types of seals being developed, describe unique test techniques used to assess seal performance, and present leakage flow data under representative pressure, temperature, and scrubbing conditions. Feasibility of the braided rope seals for both an industrial tube seal and a turbine vane seal application is also demonstrated.**

## Introduction

AIRCRAFT engine turbine inlet temperatures and industrial system temperatures continue to climb to meet aggressive cycle thermal efficiency goals. Advanced material systems including monolithic/composite ceramics, intermetallic alloys (i.e., nickel aluminide), and carbon–carbon composites are being explored to meet aggressive temperature, durability, and weight requirements. Incorporating these materials in the high-temperature locations in the system, designers must overcome materials issues such as differences in thermal expansion rates and lack of material ductility.

Designers are finding that one way to avoid cracking and buckling of the high-temperature brittle components rigidly mounted in their support structures is to allow relative motion between the primary and supporting components. Often, this joint occurs in a location where differential pressures exist, requiring high-temperature seals. These seals or packings must exhibit the following important properties: operate hot (>1300°F), exhibit low leakage, resist mechanical scrubbing caused by differential thermal growth and acoustic loads, seal complex geometries, retain resilience after cycling, and support structural loads.

### Background

Rope packings can be traced back to the early days of the industrial revolution to seal stuffing boxes and valves to prevent excessive leakage. An excellent summary of types of rope seal packings is given in Mathews and McKillop.[1] As engine temperatures continued to rise, novel adaptation of these seal packings were required to meet modern turbine engine and hypersonic engine requirements. Previous programs endeavored to develop high-temperature (≥1500°F), high-pressure (up to 100 psi), flexible seals to meet aggressive sealing goals of ramjet/scramjet engines considered for future hypersonic vehicles; for example, the National Aerospace Plane (NASP). The braided all-ceramic and hybrid seals were developed to operate hot, maintain resiliency, and resist scrubbing damage over the life of the hypersonic engines. Steinetz et al.[2] reports on the durability and flow resistance of both seals at temperatures up to 1500°F. The all-ceramic seal survived about one-half of the sliding duty cycle, and the hybrid braided rope seal survived the full sliding duty cycle anticipated for the hypersonic engine. The duty cycle in these earlier applications far exceeded those required herein. Models for predicting leakage

Presented as Paper 96-2910 at the AIAA/ASME/SAE/ASEE 32nd Joint Propulsion Conference, Lake Buena Vista, FL, July 1–3, 1996; received July 12, 1996; revision received April 6, 1997; accepted for publication April 8, 1997. 

*Senior Research Engineer, Structural Dynamics Branch. Member AIAA.

†Research Engineer, NASA Lewis Research Center, 21000 Brook Park Road, M/S 23-3, Cleveland, OH 44135. Member AIAA.

‡Research Engineer, Fatigue and Fracture Branch.

§Principal Engineer, Engineering Materials Department.

¶Staff Engineer, Demonstration Engine Systems Department; currently at Northern Research and Engineering Corporation, Woburn, MA 01801.

flow through these porous structures are reported in Cai et al.[3,4] and Mutharasan et al.[5]

The feasibility of applying braided rope seals for both an industrial and turbine vane seal application was investigated in this study.

### Industrial Tube Seal

In the industrial tube seal application, a seal is designed to serve as a seal and a compliant mount, allowing relative thermal growth between the high-temperature, low-expansion rate primary structure and a higher expansion rate structural support preventing excessive thermal strains and stresses. Two seals were examined for this study. The first all-ceramic seal consists of a tightly packed ceramic core overbraided with a ceramic sheath for low-leakage, low-scrubbing environments. The second hybrid seal consists of a tightly packed ceramic core overbraided with a superalloy wire sheath, and was tested as an abrasion-resistant alternative.

### Turbine Vane Seal

Designers are pursuing advanced material systems to meet high rotor inlet temperatures and minimize cooling requirements. Nickel aluminide (NiAl) is an attractive material system for high-temperature engine structural applications.[6] Key advantages over conventional superalloys include: low density, 0.21 lbm/in.$^3$ is approximately two-thirds that of superalloys; high-temperature oxidation resistance; high melting point, approximately 400°F higher than conventional nickel-based superalloys; and very high thermal conductivity, approximately 3–8 times that of conventional superalloy materials. Because of the higher conductivity, the temperature distribution in a NiAl turbine blade is more uniform, and the life-limiting hot-spot temperatures are reduced by as much as 100°F. Constraining factors in applying NiAl are its limited fracture toughness (4.6–7.3 ksi$\sqrt{\text{in.}}$) and very low tensile ductility, 0–2% (depending on composition and orientation), which are substantially less than conventional cast vane alloys. These material limitations require special design techniques to prevent thermal fracture and ensure a successful design.

Conventional turbine vanes are cast and furnace brazed to the inner and outer nozzle shrouds. It was discovered through early flame tests that brazed NiAl vanes could not withstand a sudden thermal shock. A more novel attachment technique, as discussed in this paper, was required to permit vane thermal expansion/contraction without fracture.

The objective of this study is to present ambient compression measurements and flow measurements under simulated pressures, temperatures, and scrubbing conditions for small diameter (1/16- and 1/8-in.) seals. Feasibility of the braided rope seals for both a turbine vane seal and an industrial tube seal application is also demonstrated.

## Test Apparatus

### Flow Tests

Flow experiments were performed on braided rope seals in a high-temperature flow and durability test rig, shown schematically in Fig. 1. Test seals with a length of 7.80 ± 0.05 in. were mounted in the grooves of the piston, and the piston/seal assembly was inserted into the cylinder. The free ends of the seals were joined together in the groove by means of a short lap joint. Preload was applied to the seals through a known interference fit between the seal and the cylinder i.d. Preload was varied by mounting stainless-steel shims in the piston groove under the seal. During flow testing, hot pressurized air entered at the base of the cylinder and flowed to the test seal that sealed the annulus created by the cylinder and piston walls. For all tests, the piston-to-cylinder radial gap was 0.007 in. The Inconel X-750 test fixture is capable of testing seal flow and durability at temperatures between 70–1500°F, pressures between 0–95 psig, and flows between 0–3.5 standard cubic feet (air) per minute (SCFM).

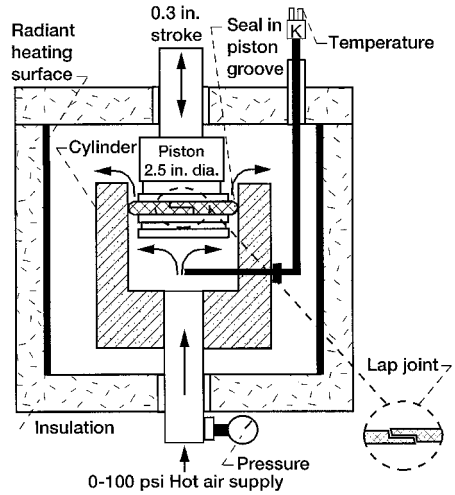


**Fig. 1 Schematic of flow fixture.**

At high temperatures, the durability of the test seals was investigated by reciprocating the piston within the stationary cylinder. Piston stroke movements of 0.3 in. were used in these tests to simulate anticipated relative thermal growths. Movement of the piston is guided by preloaded precision linear bearings.

The rig is externally heated by two 3.4-Btu/h (1-kW) ceramic fiber radiant heaters (Fig. 1). Both heaters are in the shape of a semicylindrical shell with the inside surfaces being heated. When clamped together, the ceramic fiber heaters form a continuous, radiating heating surface around the rig's cylinder and piston. Radiant heater temperatures were set about 70°F above the required operating temperature to overcome radiant losses. The heaters, cylinder, and piston are surrounded by 2-in.-thick alumina board insulation to minimize heat losses.

Before the pressurized air enters the cylinder, it is heated by several electric resistance heaters. First, the air flows through a 3.9-Btu/h (1.15-kW) primary air heater. Maximum sheath temperature of the air heater is 1650°F, and the plumbing surrounding the heater is encased in rigid alumina insulation. The air supply tubing between the air heater and the cylinder is wrapped with three 3.4-Btu/h (1-kW) flexible cable heaters. The cable heaters, capable of 1600°F, are wrapped externally with flexible alumina insulation. The cable heater arrangement not only serves to eliminate heat loss through the plumbing downstream of the tubular heater, but if needed, it can also boost the air supply temperature. All joints are certified as leak-tight prior to a run.

During flow experiments, all temperature, pressure, and flow data were continuously monitored at 10 samples per second using a 486 personal computer, with a 12-bit A/D conversion board and commercially available data acquisition software (Labtech Notebook). The temperature and pressure of the hot flow gas were measured immediately upstream of the test seal (Fig. 1). Temperature measurements were made using K-type thermocouples with an accuracy of ±0.75% of the reading. Pressure was measured as the differential between the upstream flow pressure and atmospheric (ambient) pressure downstream of the test seal using a variable capacitance pressure transducer (accuracy of ±0.14% full scale, full scale of 100 psi). The air mass flow through the seal was measured upstream of the air heaters, where measurements could be taken at room temperature with thermal mass flow meters. Volumetric flow was obtained by multiplying the mass flow by air density at room temperature. A 0–0.35 SCFM range flow meter with ±0.25% full-scale accuracy was used to measure low flows. All other flow measurements were taken with a 0–3.5 SCFM range flow meter with ±1% of full-scale accuracy.

*Thermal Growth*

During data collection, special care was taken to monitor the relative thermal growth between the piston and the cylinder. The cylinder outer wall temperature and the piston inner wall temperature (the piston is hollow) were monitored, and flow data were collected only when the temperature differential between these surfaces was less than 40°F. At operating conditions, a 40°F temperature differential results in no more than 0.0005 in. relative radial growth of the cylinder surface away from the piston surface.

Thermal growth differential also exists between the ceramic-based seal and the superalloy piston. As the piston circumferentially outgrows the seal, the seal ends move apart. To account for this, the seal free ends were joined together as a lap joint (Fig. 1). The lap joint prevents a free-flow path from occurring. A lap joint 3/32 in. in minimum length was used to prevent joint opening and to mitigate the effects of 1/16 in. in relative piston-to-seal differential circumferential growth.

**Compression Tests**

Experiments were conducted to determine the preload behavior of seals with respect to the linear crush applied to the seals. Seal preload behavior was measured at room temperature during compressive loading, using a compression/tension test fixture set up for compression only (Fig. 2). Seals were loaded into the grooved seal holder. The amount of seal compression was measured using a linear variable differential transducer (LVDT, ±0.0001 in. accuracy), monitoring the movement of the seal holder relative to a zero condition established with the top and bottom surfaces set in mating contact. Average compressive load (and, hence, preload) was calculated by dividing the measured compressive force during loading by the contact area left on the pressure-sensitive film.

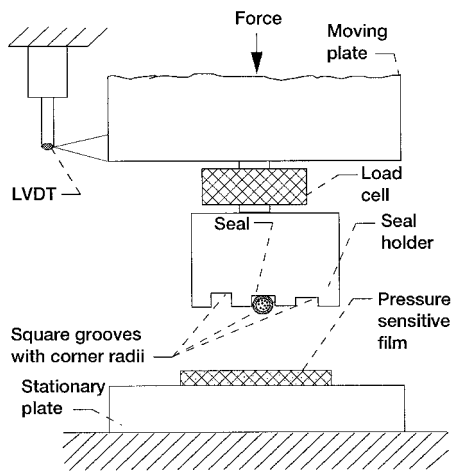


**Fig. 2 Schematic of compression fixture.**

The compression loads (lb) and pressures (psi) herein are correct, and have been substantiated with a separate compression system.

A pressure-sensitive film was mounted on the lower stationary plate such that the seal would contact only the film when the seal holder/moving plate assembly was moved into preload contact. The film color develops under compressive loading; therefore, the seal leaves a footprint after it has been crushed against the stationary plate. The pressure-sensitive film begins to develop color under compressive loads greater than or equal to 28 psi, and the shade of the developed film becomes darker as the load is increased. At seal contact pressures greater than or equal to 100 psi, the developed color is dark enough to reliably measure the dimensions of the contact area. Contact width was measured using a dial vernier caliper in several locations along the 4-in.-long specimen. Variations in contact width measurement were minimized by averaging multiple measurements.

To determine the accuracy of the width and length measurements, experiments were performed using the compression test fixture, in which a rigid object of known width and length was compressed against pressure-sensitive film samples. For applied preloads of 100 psi and greater, measured footprint widths and lengths on the film were within ±0.001 in. of the actual width and length of the object. Load cell accuracy (200 lb range) was ±0.50% of full scale. Overall accuracy of preload values, i.e., contact pressure, was calculated to be ±3.4% of the value.[7]

**Seal Specimens**

*Industrial Tube Seal Application*

The all-ceramic rope seal was tested as the primary seal for the industrial tube seal application. The all-ceramic rope seal consists of a dense uniaxial core of ceramic fibers overbraided with a two-layer ceramic sheath. These seals were selected for several reasons. The Nextel 550 fibers can operate to 2000°F continuously (2200+°F short term), and they are much more inert and resist abrasion than either the Nextel 312 or 440 fibers.[8] Small, $3.2 \times 10^{-4}$ in. (8 $\mu$m) Nextel 550 fibers were selected for both the core and the sheath to minimize leakage through the seal and between the sheath and adjacent surfaces. Table 1 gives details of the seal sheath, core construction, and specific materials. A hybrid seal discussed later in this paper was also tested as an abrasion-resistant alternative.

Differential expansion between the industrial tube (low coefficient of thermal expansion) and seal-holding fixture was estimated to be 0.3 in.. Seal feasibility would be demonstrated if the seal flow was less than or equal to the flow goal (0.0064 SCFM/in. seal for a 2 psid pressure), and durability was acceptable after 10 cycles.

*Turbine Vane Seal Application*

For the turbine vane seal application, a hybrid seal was used, consisting of a dense uniaxial core of Nextel 550 fibers over-

**Table 1 Braided rope seal construction matrix**

| | | Core | | | | Sheath | | | | | | |
|---|---|---|---|---|---|---|---|---|---|---|---|---|
| Seal | Diameter, in. | Material[a] | Denier | Fiber diameter, in.[b] | Number of yarns | Material[a,c] | Denier | Fiber diameter, in.[b] | Number of layers | Number of filaments or yarns per tow | Braid angle $\theta$, deg | Number of carriers |
| All-ceramic: | | | | | | | | | | | | |
| NTWAC-1 | 0.064 | NX550 | 700 | $3.2 \times 10^{-4}$ | 15 | NX550 | 700 | $3.2 \times 10^{-4}$ | 2 | 1 | 30 | 4.8 |
| NTWAC-2 | 0.124 | NX550 | 700 | $3.2 \times 10^{-4}$ | 109 | NX550 | 700 | $3.2 \times 10^{-4}$ | 2 | 1 | 45 | 8.8 |
| Hybrid: | | | | | | | | | | | | |
| NTWHY-1 | 0.060 | NX550 | 700 | $3.2 \times 10^{-4}$ | 35 | HS188 | 110 | $1.6 \times 10^{-3}$ | 1 | 10 | 46 | 12 |

[a]Ceramic fiber composition by weight percentage: NX550 (Nextel 550): 73 $Al_2O_3$, 27 $SiO_2$.
[b]$1 \times 10^{-3}$ in. = 25 $\mu$m.
[c]Metal wire composition by weight percentage: HS188 (Haynes 188): 38 Co, 22 Cr, 14 W, 3 Fe, 1.25 Mn, 0.5 Si, 0.08 La, 0.015 B, 0.05 C.

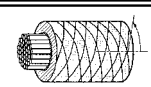

braided with a single sheath layer composed of yarns made of 0.0016 in. (40 $\mu$m) Haynes 188 wires. Hybrid seals were selected for this application to resist scrubbing damage against a rough thermal barrier coating and to resist potential damage from acoustic-induced fretting at 1500+°F. Fine diameter sheath wires were used to minimize sheath leakage.

The relative vane-to-seal thermal growth over one thermal cycle was estimated to be 0.04 in. To ensure durability in the harsher engine environment, the same 10 cycles of 0.3 in. were used to examine durability of the vane seal at 1500°F. Durability cycles were run at two linear compressions of 0.018 and 0.020 in., approximating the nominal 0.022-in. linear seal crush in the actual application. Room-temperature compression tests revealed 0.018- and 0.020-in. linear compressions resulting in 500- and 675-psi seal contact pressures, respectively. Design calculations indicated that with pressure loads, the vane would move toward the suction side of the blade by 0.002 in. Depending on location around the vane perimeter, the seal would experience compressions of 0.020 in. (pressure side), 0.022 in. (centerline), or 0.024 in. (suction side).

## Test Procedures

### Flow Tests

Seal flow data for the industrial tube seal application were collected before and after scrubbing (10 cycles of 0.3-in. linear stroke at 1300°F), at temperatures of 70, 900, 1100, and 1300°F, and at pressures of 2, 5, and 10 psid. Data were also collected for specific seal builds at higher differential air pressures of 20, 40, 60, 80, and 95 psid. Primary and repeat flow tests were performed on 1/16 in. and 1/8 in. diam all-ceramic seal specimens for preloads of 100, 110, 150, and 250 psi. Primary and repeat flow tests were performed on the 1/16-in.-diam hybrid seals for preloads of 150 and 250 psi.

For the turbine vane seal application, flow tests were performed on 1/16-in.-diam hybrid seal specimens for nominal preloads of 500 and 675 psi. Flow data was collected at three temperatures (70, 1300, and 1500°F), eight pressures (2, 5, 10, 20, 40, 60, 80, and 95 psid), and two scrubbing conditions (no scrubbing and 10 cycles of 0.3 in. scrubbing at 1500°F). After all flow experiments, the piston was retracted and the seal sample examined, and the seal overhang was measured to verify the validity of the compression testing procedure.

### Compression Tests

Compression tests were performed on all-ceramic seals to determine required linear crushes for 100, 110, 150, and 250 psi nominal preloads for both all-ceramic seal sizes, and 150, 250, 500, and 675 psi nominal preload for the 1/16-in.-diam hybrid seal. The 500 and 675 psi nominal preload experiments were performed in support of the turbine vane seal application.

A test procedure was developed using the compression testing fixture to accurately simulate the loading conditions in the flow test fixture. Preliminary compression experiments had revealed that the seals have a hysteresis, or nonrecoverable displacement after loading. Therefore, accurate simulation of flow fixture conditions during compression testing was essential to determine preload.

In the flow fixture, a particular linear crush (equal to the seal and cylinder interference) is consistently applied to the seal specimen throughout a series of experiments. For a static condition, the seal will be acted upon by a compressive force, the preload force, that is normal to the cylinder and piston surfaces. Through successive or continuous loading, this preload force will drop as the seal settles into its final operating condition. To duplicate this drop during compression experiments, the seal was crushed with the compression test fixture to the same displacement (corresponding to a known interference) during each loading cycle. At this displacement, the normal force acting on the seal is considered the preload force.

Because of sliding conditions (installation and cycling) in the flow test fixture, both a normal and a frictional force are exerted on the seal, causing the seal to settle in the groove. The friction force acts tangentially between the seal and the cylinder wall surfaces. Previous work with ceramic rope seals[2] indicated that the friction coefficient is generally large ($\mu$ = 0.6–1.0); therefore, both the normal and friction force must be considered for accurate modeling of this additional loading of the seal. To accomplish this, a friction coefficient of $\mu = 1$ was chosen, and the magnitude of the vector sum of the preloading force and the frictional force was applied to the seal at the end of each displacement load cycle. This applied force equals the preloading force (measured at the known interference) multiplied by a factor of 1.4, i.e., Force $\times \sqrt{2}$.

This loading procedure was repeated for at least three cycles to remove seal hysteresis. Preload was determined from the last (generally third) loading cycle after the majority of hysteresis had been removed. Using the last cycle, compression data ensures that the seal will experience this preload after settling has occurred. This compression procedure was validated using seal overhang or residual-interference measurements collected in the flow fixture after the flow tests. After each test, the amount that the seal extended radially out of the piston groove was measured. This measurement gauges the seal's compression-set, or conversely, the retained seal interference; for example, preload, when loaded into the cylinder. The seal overhang data agreed to within 0.001 in. to that expected from the last cycle compression data.

## Results and Discussion

### Industrial Tube Seals

*Flow Results*

Table 2 summarizes all-ceramic seal and hybrid seal flow rates, and shows postscrubbing results (10 cycles of 0.3 in. scrubbing at 1300°F) for both primary and repeat tests for the 2-psid industrial tube seal pressure. Figures 3–5 present average flow vs pressure data for four temperatures (70, 900, 1100, and 1300°F), after scrubbing (10 cycles of 0.3-in. scrubbing at 1300°F), at 250 psi nominal preload. For clarity, error bars ($\pm 2\sigma$) are shown for the 70 and 1300°F plots only. Flow results for the 1/16- and 1/8-in. all-ceramic seals exhibited good repeatability at preloads greater than or equal to 110 psi (Table 2). Furthermore, flow rates for the all-ceramic seals decreased with increasing preload. The 1/16-in.-diam all-ceramic seal flow rates were less than the 1/8-in.-diam all-ceramic seal flow rates for the same preload conditions (Table 2). This observation may be attributed to a more uniform footprint between the 1/16-in.-diam seal and adjacent surfaces, as evidenced in the compression tests discussed later in this paper.

The 1/16-in. hybrid seals exhibited good repeatability at 150 and 250 psi nominal preload. Hybrid seal flow decreased with increasing temperature at all preloads and for all temperature conditions.

*Effect of temperature.* For all seals, the flow rates at elevated temperatures were significantly lower than flow rates at room temperature, with the exception of the 100 psi preload condition. Gas viscosity increases with temperature ($\mu \propto T^{2/3}$), which suggests that flow will decrease with temperature. However, in some instances for all-ceramic seals, flow did increase between the 900 and 1300°F data sets. This behavior may be attributed to the thermal growth differential between the piston circumference and the seal length (the piston outgrows the seal circumferentially by approximately 1/16 in.). This relative motion of the seal ends away from each other at the lap joint may allow for increased leakage at the joint, even though an overlap joint of 3/32 in. was used. This effect is mitigated with increasing preload, and may be eliminated if the thermal growth coefficients of the seal's housing and the seal are more similar. The trend of increasing flow with increasing temperature for the 100 psi preload condition may be because of leakage through the joint, as mentioned earlier. It is possible that with the lower preload, the seal may slip easier in the groove, thus facilitating the opening of such a region in the joint.

**Table 2 All-ceramic (1/16- and 1/8-in.) and hybrid (1/16-in.) seal flows at operating temperature for several preloads at 2 psid pressure**

| Seal type | Seal diameter, in. | Preload, psi | Linear crush, in. | Flow, SCFM/in. At 1100°F | Flow, SCFM/in. At 1300°F | Flow goal, SCFM/in. |
|---|---|---|---|---|---|---|
| All-ceramic | 0.064 | 100 | 0.005 | 0.149 | 0.149 | 0.0064 |
| All-ceramic | 0.064 | 100 | 0.005 | 0.072 | 0.091 | |
| All-ceramic | 0.060 | 110 | 0.013 | 0.0064 | 0.0068 | 0.0064 |
| All-ceramic | 0.060 | 110 | 0.013 | 0.0064 | 0.0073 | |
| All-ceramic | 0.064 | 150 | 0.015 | 0.0038 | 0.0040 | 0.0064 |
| All-ceramic | 0.064 | 250 | 0.018 | 0.0023 | 0.0024 | 0.0064 |
| All-ceramic | 0.064 | 250 | 0.018 | 0.0022 | 0.0020 | |
| All-ceramic | 0.124 | 100 | 0.008 | 0.112 | 0.151 | 0.0064 |
| All-ceramic | 0.124 | 100 | 0.008 | 0.085 | 0.120 | |
| All-ceramic | 0.120 | 110 | 0.021 | 0.0092 | 0.010 | 0.0064 |
| All-ceramic | 0.124 | 150 | 0.031 | 0.0086 | 0.0076 | 0.0064 |
| All-ceramic | 0.124 | 150 | 0.031 | 0.0096 | 0.0080 | |
| All-ceramic | 0.124 | 260 | 0.037 | 0.0040 | 0.0036 | 0.0064 |
| All-ceramic | 0.124 | 260 | 0.037 | 0.0039 | 0.0031 | |
| Hybrid | 0.060 | 150 | 0.011 | 0.0107 | 0.0096 | 0.0064 |
| Hybrid | 0.060 | 150 | 0.011 | 0.0123 | 0.0114 | |
| Hybrid | 0.060 | 250 | 0.014 | 0.0070 | 0.0064 | 0.0064 |
| Hybrid | 0.060 | 250 | 0.014 | 0.0066 | 0.0063 | |

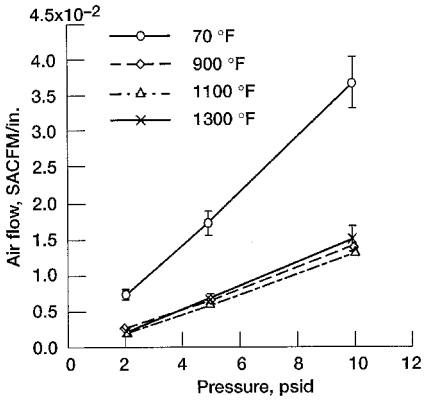


**Fig. 3 Flow vs pressure data for four temperatures, 1/16-in.-diam all-ceramic seal, 250 psi preload, after scrubbing.**

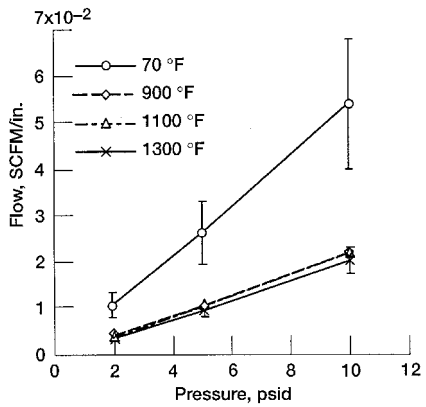


**Fig. 4 Flow vs pressure data for four temperatures, 1/8-in.-diam all-ceramic seal, 250 psi preload, after scrubbing.**

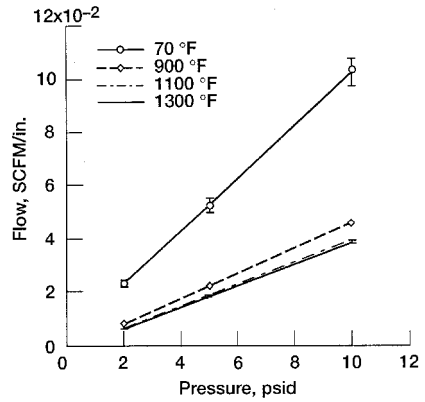


**Fig. 5 Flow vs pressure data for four temperatures, 1/16-in.-diam hybrid seal, 250 psi preload, after scrubbing.**

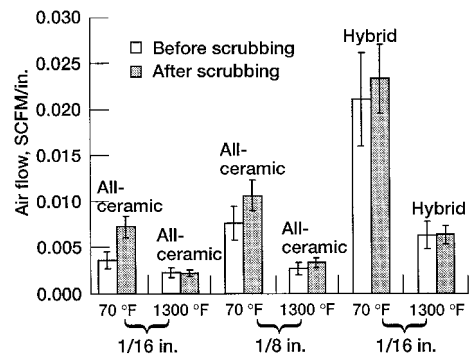


**Fig. 6 Effect of scrubbing and temperature on seal flow; D$p$ = 2 psid; 250 psi preload; 1/16- and 1/8-in. all-ceramic seals and 1/16-in. hybrid seals.**

*Effect of hot scrubbing.* Seal flow increased only slightly after hot scrubbing for all preload conditions (Fig. 6). Sheath damage was generally minor for all cases (Fig. 7). Away from the joint, the sheath was intact and showed only minor fiber breakage. The initial 1/8-in.-diam all-ceramic seal (at 250 psi nominal preload) showed small localized sheath fraying (approximately 1/4 in. long at two locations). This initial 1/8-in. seal was installed with only the aid of the lead-in chamfer on the cylinder. The 1/8-in. all-ceramic 250 psi preload repeat seal was installed with a clamping fixture during insertion of the seal/piston into the cylinder, eliminating sheath fraying. Hybrid seals resisted abrasion very well. Figure 8 shows a close-up of the hybrid seal lap joint after 10 cycles of 0.3 in. scrubbing at 1300°F. The seal sheath was not damaged away from the lap joint. Some minor wire bending is noticed at the joint.

*Comparison to flow goal.* Examining Table 2, the 1/16-in.-diam all-ceramic seals met the flow goal of 0.0064 SCFM/in. seal for 150 and 250 psi preloads and marginally met the goal at 110 psi. The flow goal was arrived at a priori to aid in selecting seals to minimize system purge requirements. The 1/8-in.-diam seals exhibited higher leakage, but met the flow

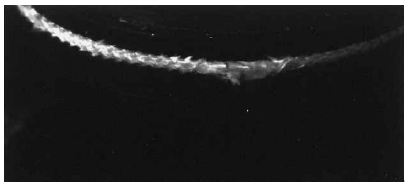

**Fig. 7 1/16-in.-diam all-ceramic seal after scrubbing, 250 psi preload.**

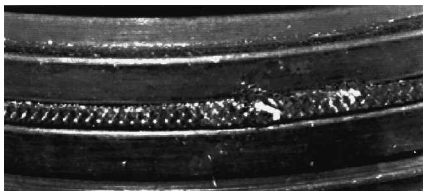

**Fig. 8 1/16-in. hybrid seal after scrubbing, 250 psi preload.**

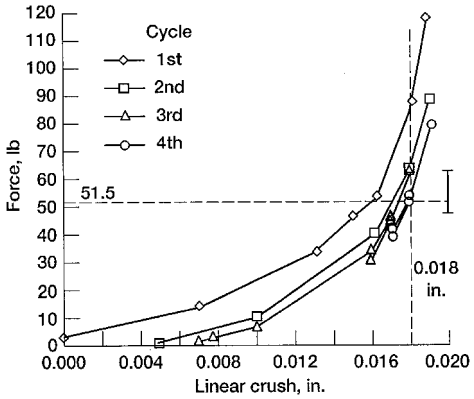


**Fig. 9 Preload vs linear compression data, 1/16-in.-diam all-ceramic seal, 250 psi preload (6 2$s$ uncertainty shown at design point).**

goal at 260 psi preload. Other tests could be done with the 1/8-in. seal to determine threshold preloads where the seal would meet the flow goal. Low preload is preferred in the industrial application for design considerations. The 1/16-in.-diam hybrid seal met the flow goal at 250 psi preload. The seal flows met the flow goals for the design preloads, 150 and 250 psi. Furthermore, sheath damage was minimal over the thermal cycles. Based on these observations, the braided seal is deemed feasible for the industrial tube seal application.

*Compression Results*

Figure 9 shows the force vs linear crush characteristics of the 1/16-in.-diam all-ceramic seal at 250 psi nominal preload (the data are qualitatively representative of the 1/8-in. seal force vs linear compression data). Figure 10 shows the force vs linear crush characteristics for the 1/16-in. hybrid seal at 250 psi nominal preload. Figures 9 and 10 show $\pm 2\sigma$ error bars for the design point only. Data shown in Figs. 9 and 10 are for one of two tests, and the error bars are placed to reflect the mean of the two data sets. For all seals tested and for all preloads, the last two load vs crush lines are very close in value, indicating that the majority of seal hysteresis was removed prior to preload determination.

During a compression experiment, the seal sample is repeatably crushed to the same linear displacement. The footprint width of the last load cycle is used in conjunction with the measured force vs crush information, to estimate the preload that corresponds to the repeated linear crush value. Figure 11 shows the relationship between the linear crush value and measured seal preload for 1/16-in. all-ceramic seals (again, this data is qualitatively representative of the data for the 1/8-in.-

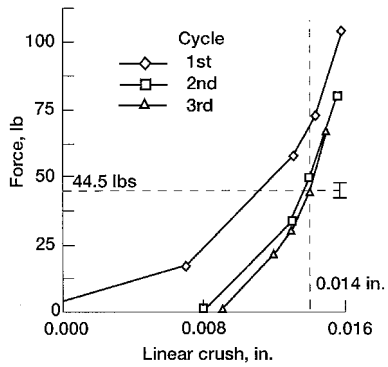


**Fig. 10 Preload vs linear compression data, 1/16-in.-diam hybrid seal, 250 psi preload (6 2$s$ uncertainty shown at design point).**

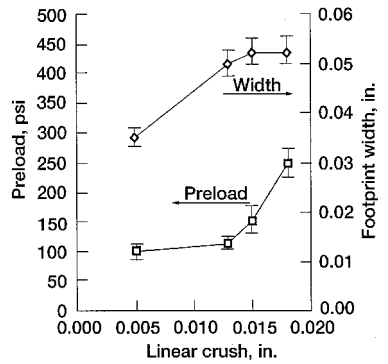


**Fig. 11 Footprint width and preload vs linear compression for 1/16-in.-diam all-ceramic seals.**

diam seals). Generally, there is a plateau in their characteristic preload vs crush curve. The plateau exists because seal contact width increases with force, resulting in very little net change in preload value. This plateau indicates that for both the 1/16- and 1/8-in.-diam all-ceramic seals there is a range of linear crush in which preload does not significantly change, but seal flow (Table 2) changes by approximately one order of magnitude. At higher linear crushes, the plateau behavior disappears when the increase in force per unit of linear crush exceeds the increase in footprint width per unit of linear crush. The footprint width asymptotically reaches a maximum, and at that point the net preload increases sharply with linear crush.

While unit preload may not change radically along this plateau, the seal's resiliency; for example, the ability to track distortions, is greatly increased. This point can be illustrated by examining the amount of distortion, or working deflection, the seal can follow while maintaining 50% or more of the seal's contact force. Table 3 compares the seal's working deflection for this criterion for the 1/16- and 1/8-in. seals for 100, 110, and 250 psi nominal preloads.

As Table 3 illustrates, the seal's resiliency, or working deflection, doubles (0.0015 to 0.003 in.), when increasing the unit preload from 100 to 110 psi nominal, and it more than doubles when increasing the unit preload from 100 to 250 psi. This clearly increases the seal's ability to accommodate differential growths and manufacturing tolerances.

*Footprint Observations*

*All-ceramic seals.* Compression experiments not only produce preload information, but they also produce visual evidence of seal footprints. After the pressure-sensitive film develops under a preloaded seal, observations can be made regarding the quality and continuity of the seal contact with its mating surfaces. At approximately 100 psi, seal contact for both sizes of all-ceramic seals is intermittent with large gaps between the areas in loaded contact. Note that the pressure-sensitive film develops at preloads of 28 psi and greater. Some

**Table 3 All-ceramic seal working deflection for criteria that seal maintains 50% or more of design preload[a]**

| Seal diameter, in. | 100 psi nominal base, in. | 110 psi vs base: Design preload, 110 psi nominal | 110 psi vs base: Increase in working deflection | 250 psi vs base: Design preload, 250 psi nominal | 250 psi vs base: Increase in working deflection |
|---|---|---|---|---|---|
| 1/16 | 0.0015 | 0.003 | 2× | 0.004 | 2.6× |
| 1/8 | 0.002 | 0.005 | 2.5× | 0.005 | 2.5× |

[a]Last load cycle data.

**Table 4 All-ceramic and hybrid seal measured contact widths[a]**

| Seal type | Preload, psi nominal | Linear crush, in. | Contact width, in. |
|---|---|---|---|
| All-ceramic, 1/16 in. diameter | 100 | 0.005 | 0.034 |
| | 110 | 0.013 | 0.050 |
| | 150 | 0.015 | 0.052 |
| | 250 | 0.018 | 0.052 |
| All-ceramic, 1/8 in. diameter | 100 | 0.008 | 0.041 |
| | 110 | 0.021 | 0.053 |
| | 150 | 0.031 | 0.077 |
| | 250 | 0.037 | 0.078 |
| Hybrid, 1/16 in. diameter | 150 | 0.011 | 0.042 |
| | 250 | 0.014 | 0.043 |
| | 500 | 0.018 | 0.053 |
| | 675 | 0.020 | 0.056 |

[a]Last load cycle data.

of the undeveloped regions could be in contact, but not at a high enough preload to develop. However, we believe from the high-flow results (Table 2) for the 100 psi preload, that there are some thin open areas between the seal and piston that are leak paths.

At approximately 110-psi preload, the 1/16-in. all-ceramic seal footprint is almost continuous, and the 1/8-in. all-ceramic seal footprint is more continuous, but still somewhat intermittent. At approximately 250 psi preload, the 1/16-in. all-ceramic seal footprint is very solid and continuous. This solid contact eliminates flow paths between the walls and the seal, thus further reducing overall seal leakage. The 1/8-in. seal footprint at approximately 250 psi exhibits some intermittency, but more seal is in contact at this preload than at lighter preloads. Footprint widths were measured from these film samples, and these measured contact widths (obtained after the last load cycle) are summarized for each seal in Table 4.

*Hybrid seals.* At all measured preloads, the hybrid seal footprint is solid and continuous. This solid contact eliminates flow paths between the walls and the seal, thus reducing overall seal leakage. Measured contact widths (obtained after the last load cycle) are summarized for each seal in Table 4.

### Turbine Vane Seals

*Flow Results*

As with the previously described lower preloads, seal flow performance for the hybrid seals did not appreciably degrade after hot scrubbing at elevated temperatures for the 500 and 675 psi nominal preload conditions. Seal flow was linearly dependent on pressure (2–95 psid). After scrubbing, the seal sheath was not damaged, and only minor wire bending was noticed at the lap joint. Additionally, the flow decreased with increasing temperature at both the 500 and 675 psi nominal preload conditions.

A synopsis of flow results (after hot scrubbing) for the vane seal application showing the effects of temperature, pressure, and preload on the seal flow is shown in Fig. 12. No repeat data sets were collected, therefore, Fig. 12 contains no error bars. At 1500°F and operating pressure of 95 psid, increasing

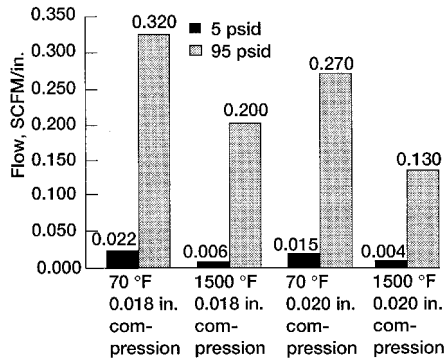


**Fig. 12 Effect of temperature, pressure, and representative compression on seal flow after cycling for 0.060-in. hybrid vane seal.**

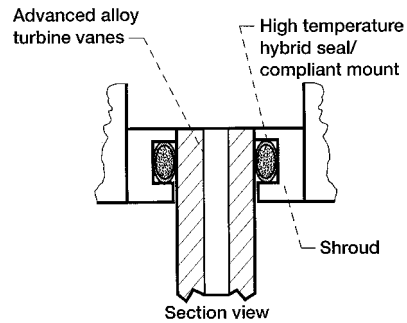


**Fig. 13 Schematic of vane seal hardware.**

the preload from 0.018- to 0.020-in. compression reduced leakage by one-third.

*Vane Seal Application Specifics*

*Geometry.* Through discussions, General Electric (GE) and NASA arrived at a vane attachment technique indicated in Fig. 13. The turbine vane is sealed and supported at the outer shroud location, using a preloaded hybrid seal of the type described herein. The seal acts as a compliant mount supporting aerodynamic loads and allows the vane to grow in the spanwise (e.g., radially outward) direction during heat-up and cooldown without excessive thermal stress. The seal also minimizes leakage of coolant bleed air past the seal into the turbine, thereby minimizing parasitic thermal efficiency losses.

*Installed performance.* GE demonstrated feasibility of the compliant vane seal/mount technique through both flame tunnel (thermal shock) and combustor tests. Test success was based on the vane surviving the test without thermal cracking, as the seal allowed the vane to float freely while still sealing (leak rates were not measured). The vane and seal survived about one dozen hot cycles in the combustor test. These tests qualified the design for subsequent tests in the Integrated High Performance Turbine Engine Technology (IHPTET) Joint Technology Advanced Gas Generator (JTAGG) test engine. The NiAl vane and seal were implemented into the JTAGG engine and successfully run for multiple cycles, meeting the following seal performance criteria: operate at temperatures up to 1500°F and pressures up to 100 psid, allow the vane to slide

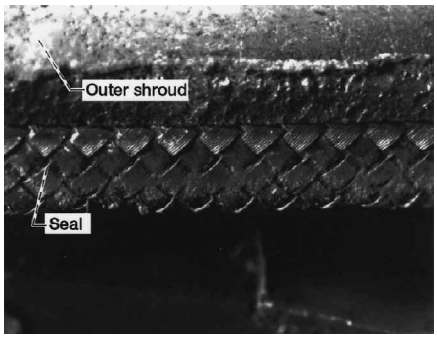


**Fig. 14 Close-up (14× magnification) of turbine vane seal after engine testing showing no damage.**

0.06 in. relative to the mount without vane fracture, and exhibit low seal wear. The seal enabled the vane to operate at IHPTET Phase 1 rotor–inlet temperatures (classified), and this technology combined with others contributed to meeting JTAGG Phase 1 program goals, which included a 20% reduction in specific fuel consumption and a 40% increase in power-to-weight ratio in a 4000–6000-eshp-class turboprop/turboshaft engine.[9] Figure 14 shows a close-up of the vane seal hardware after engine testing, showing no thermal distress or seal–fiber breakage. The vane exhibited no thermal cracking and met all design goals. The seal operated at temperatures of 1500+°F and allowed relative vane-to-holder movement, as evidenced by trace-scrubbing marks left on the hardware.

## Summary and Conclusions

As operating temperatures of advanced gas turbine and industrial systems continue to rise, designers face more difficult challenges of implementing high-temperature structural materials and seals to meet system performance goals. To maximize efficiency, coolant flows are being reduced to their practical minimum, requiring low-leakage seals made of temperature-resistant superalloy and ceramic materials. Seals are being designed to both seal and serve as compliant mounts, allowing for relative thermal growths between high temperature, but brittle, primary structures and the surrounding support structures.

High-temperature flow and durability performances were measured for both the all-ceramic and hybrid seals for the industrial tube seal and turbine vane seal applications. Compression tests in displacement control mode were used in conjunction with pressure-sensitive film to determine seal contact pressures to establish required groove-depths to set seal preload. Displacement control mode was used to simulate the fixed interference condition that the seals experience, both in the flow fixture and the actual application. Braided seals exhibit hysteresis; for example, nonrecoverable displacement, during loading, and have a memory of previous loading conditions. It was found that testing in displacement control mode better simulated installed loading history and provided more accurate preload information than force control mode compression testing. The compression test technique was corroborated using seal-overhang/residual-interference measurements made after hot tests in the flow fixture, and showed very good agreement.

Based on the tests discussed herein, the following observations are made:

1) The 1/16- and 1/8-in.-diam all-ceramic rope seals met the flow goal and exhibited good durability for the design preloads, pressures, and operating temperatures (1300°F). Based on the screening tests performed, the feasibility of the all-ceramic rope seal has been established for the industrial tube seal application.

2) The hybrid-braided rope seal, high-temperature flow and durability tests performed herein, combined with GE's flame tunnel, combustor, and engine tests, demonstrated the feasibility of the hybrid seal/compliant mount arrangement for joining high-performance, advanced material system turbine vanes to their supporting structure, preventing thermally induced failure at metal temperatures 1500°F and higher.

## Acknowledgments

NASA acknowledges the financial support of Michael Kinsella, of U.S. Air Force Wright Laboratory, Wright–Patterson Air Force Base, Ohio. The authors acknowledge the contributions of Lawrence Kren and Tom Doeberling, NASA Lewis Research Center, and Michael Nathal, NASA; and Scott Walston, General Electric Aircraft Engines.

## References

[1]Mathews, A., and McKillop, G. R. "Compression Packings," *Machine Design Seals Reference Issue*, Penton Publishing, Cleveland, OH, March 1967, Chap. 8.

[2]Steinetz, B. M., Kren, L. A., and Cai, Z., "High Temperature Flow and Sliding Durability Assessments of Hypersonic Engine Seals," NASA TP-3483, Dec. 1994.

[3]Cai, Z., Mutharasan, R., Ko, F., and Steinetz, B. M., "Development of Hypersonic Engine Seals: Flow Effects of Preload and Engine Pressures," *Journal of Propulsion and Power*, Vol. 10, No. 6, 1994, pp. 884–889.

[4]Cai, Z., and Steinetz, B. M., "Numerical Simulation of the Leakage Flow of Textile Engine Seals," 26th International SAMPE Technical Conf., Atlanta, GA, Oct. 1994.

[5]Mutharasan, R., Steinetz, B. M., Tao, K., and Ko, F., "Development of Braided Rope Seals for Hypersonic Engine Applications: Flow Modeling," *Journal of Propulsion and Power*, Vol. 9, No. 3, 1993, pp. 456–461.

[6]Darolia, R., "NiAl for Turbine Airfoil Applications," *Structural Intermetallics, Proceedings of the 1st International Symposium on Structural Intermetallics*, The Metallurgical Society and The American Society for Materials, Sept. 1993, pp. 495–504.

[7]Doebelin, E. O., "Measurement Systems, Application and Design," McGraw–Hill, New York, 1983.

[8]DellaCorte, C., and Steinetz, B. M., "Relative Sliding Durability of Candidate High Temperature Fiber Seal Materials," NASA TM-105806, 1992.

[9]"Aerospace 95 Laureates," *Aviation Week and Space Technology*, Jan. 29, 1996, pp. 15–22.